Hindawi Publishing Corporation
International Journal of Antennas and Propagation
Volume 2015, Article ID 673536, 11 pages
http://dx.doi.org/10.1155/2015/673536

Research Article

Smart Wireless Power Transfer Operated by Time-Modulated Arrays via a Two-Step Procedure

Diego Masotti,[1] Alessandra Costanzo,[2] and Vittorio Rizzoli[1]

[1]*DEI, University of Bologna, Viale Risorgimento 2, Bologna, Italy*
[2]*DEI, University of Bologna, Via Venezia 52, Cesena, Italy*

Correspondence should be addressed to Alessandra Costanzo; alessandra.costanzo@unibo.it

Received 7 May 2015; Revised 16 July 2015; Accepted 21 July 2015

Academic Editor: Toni Björninen

The paper introduces a novel method for agile and precise wireless power transmission operated by a time-modulated array. The unique, almost real-time reconfiguration capability of these arrays is fully exploited by a two-step procedure: first, a two-element time-modulated subarray is used for localization of tagged sensors to be energized; the entire 16-element TMA then provides the power to the detected tags, by exploiting the fundamental and first-sideband harmonic radiation. An investigation on the best array architecture is carried out, showing the importance of the adopted nonlinear/full-wave computer-aided-design platform. Very promising simulated energy transfer performance of the entire nonlinear radiating system is demonstrated.

1. Introduction

Time-modulated arrays (TMAs) are extremely versatile radiating systems due to the almost unlimited possible combinations of control sequences that can be applied to periodically switch on/off the array elements [1]. Many research groups have introduced interesting potential applications of TMAs, such as sideband suppression [2–4], adaptive nulling [5], harmonic beam-steering [6, 7], and direction finding [8–10]. These and other works [11–13] propose different optimization strategies for the control sequence optimization but almost invariably assume that the radiating elements are isotropic and the switches behave ideally, while it has been demonstrated that realistic antenna properties and switch nonlinearities should be taken into account for a reliable assessment of TMA performance [14]. Some of these applications deal with the need for reduction of the sideband radiation occurring at the harmonics ($f_0 \pm hf_M$) of the fundamental frequency (f_0) due to the switch modulation frequency (f_M) [2–5]. For the purpose of the present work the applications taking advantage of the additional sideband radiation [6–10] are more appealing, and we will make use of the optimized sequence taken from literature, even if suboptimal (as demonstrated in [14]).

In this paper we intend to exploit these properties by following the rigorous approach described in [14], in order to provide a new smart wireless power transfer (WPT) functionality operated by time-modulated arrays. In the authors' opinion this could be a new promising field of application of such systems, because of the unrivaled reconfigurability offered by TMAs. It is worth noting that this is not the unique advantage of these radiating systems: they also have a much simpler architecture with respect to other available solutions, such as phased arrays and retrodirective arrays [15], since comparable scanning capabilities can be obtained without the need for phase-shifters.

The paper is organized as follows: a brief recall of TMA main features is provided in Section 2. The presence of nonlinear switches as well as of (possibly) unequally spaced radiating elements strongly suggests the use of a rigorous nonlinear/electromagnetic computer-aided-design (CAD) platform, as summarized in Section 3. The description of the whole radiating system within the CAD tool frame allows us to accurately predict the behavior of a linear TMA during the novel two-step WPT procedure, as explained in Section 4. Sections 5 and 6 provide a detailed illustration of each phase of the WPT activity, together with simulated

results for different TMA architectures, showing the high potentiality of the proposed solution.

2. Time-Modulated Array Operating Principles

In case of a linear array operating at the fundamental frequency f_0, with N elements aligned along the direction $\hat{\mathbf{a}}$ ($\hat{\mathbf{a}} \cdot \hat{\mathbf{r}} = \cos\Psi$), with interelement spacing L, the insertion of an RF switch at each antenna port allows us to introduce time-dependency in the array radiation characteristics. If each switch is driven by a periodic sequence of rectangular pulses of period $T_M = 1/f_M$, the constant complex excitation coefficients of the individual elements of a traditional array are multiplied by $U_p(t)$, representing the normalized periodic waveform operating the generic (pth) switch. The TMA far-field at the fundamental frequency f_0, evaluated at the point (r, θ, ϕ), can thus be cast in the form:

$$\begin{aligned}\mathbf{E}(r,\theta,\phi,t) &= \mathbf{E}_0(r,\theta,\phi)\sum_{p=0}^{N-1} A_p U_p(t)\, e^{jk\beta L\cos\psi} \\ &= \mathbf{E}_0(r,\theta,\phi)\,\mathrm{AF}(\theta,\phi,t),\end{aligned} \tag{1}$$

where the time-dependent array factor (AF) expression is put into evidence.

The periodicity of the sequences $U_p(t)$ biasing the switches allows us to Fourier-transform the array factor at f_0, according to the following expression:

$$\begin{aligned}\mathrm{AF}(\theta,\phi,t) &= \sum_{h=-\infty}^{\infty} \mathrm{AF}_h(\theta,\phi,t) \\ &= \sum_{h=-\infty}^{\infty} e^{j(\omega_0+h\omega_M)t}\sum_{p=0}^{N-1} A_p u_{hp} e^{jp\beta L\cos\psi}.\end{aligned} \tag{2}$$

By inspection of (2) it is straightforward to infer an interesting feature of TMA; that is, radiation takes place not only at the fundamental frequency f_0, but at sideband frequencies, $f_0 \pm hf_M$, too. This phenomenon, known as sideband radiation, represented a limitation in the first applications of these arrays [1]. The recent research activity has provided solutions to this problem, by means of proper control sequences optimization, including sideband harmonic suppression [2–4, 11]. The use of time as a further degree of freedom has paved the way to a wider spectrum of applications for this agile radiating system [5–10], because of the almost unlimited number of control sequence combinations.

For the purpose of the present paper the TMA characteristic of sideband radiation is exploited from a twofold point of view. Indeed, in Section 4 we demonstrate for the first time that the direction finding capability [8–10] in conjunction with the harmonic beam synthesis [6, 7, 16] makes the TMA architecture suitable for achieving smart far-field WPT.

3. Rigorous Simulation of Time-Modulated Arrays

As for any nonlinear system, the simulation of TMAs can be carried out by resorting to the Harmonic Balance (HB) technique [17]. According to the Piecewise HB (PHB) formulation, the circuit is divided into a linear and a nonlinear subnetwork, described in the frequency and time domains, respectively. In the TMA case these two networks are represented by the radiating array of n_A elements and the nonlinear switches, respectively. Therefore, in the simple case of one-port antennas, n_A also represents the number of ports connecting the two parts of the circuit. The PHB approach matches very well the TMA analysis needs, since a broadband full-wave analysis in the frequency domain is normally the best way to produce the rigorous description of the linear radiating portion which is essential in view of accurate simulated results [18]. On the other hand, the nonlinearities introduced by the driving diodes are easily and accurately modelled in time-domain and then Fourier-transformed into the frequency domain. The nonlinear solving system is then obtained by applying Kirchhoff's current law at all the n_A ports, for all the frequencies used in the description of the nonlinear circuit regime.

The nonlinear TMA system supports a two-tone regime consisting of the intermodulation products of the sinusoidal carrier (angular) frequency ω_0 to be radiated and the switch modulation (angular) frequency ω_M. The situation is reported in Figure 1 where time- and frequency-domain descriptions of the regime are provided.

A generic signal in the circuit can then be cast in the form

$$s(t) = \mathrm{Re}\left[\sum_{k=0}^{n_K}\sum_{h=-n_H}^{n_H} \mathbf{S}_{kh}\exp j\left[(k\omega_0 + h\omega_M)t\right]\right], \tag{3}$$

where n_K is the number of harmonics of the fundamental carrier ω_0 and n_H is the (high) number of harmonics of the modulation frequency ω_M which are needed for an accurate description of the switch nonlinear regimes and the rectangular pulse waveforms, respectively. Mainly due to the large n_H value (at least a few tens), the resulting frequency spectrum, and therefore the resulting HB solving system dimension, can be large.

The fast RF carrier (GHz) and the slow modulation frequency (up to a few MHz) may differ by several orders of magnitude. This circumstance allows the numerical analysis to be considerably simplified by resorting to the envelope-oriented PHB method [17]. According to this method the quasiperiodic two-tone regime is approximated by a sequence of fast periodic regimes (of period $T_0 = 2\pi/\omega_0$) slowly changing in time. The generic signal description (3) can then be replaced by

$$s(t_0, t_M) = \mathrm{Re}\left[\sum_{k=0}^{n_K} \mathbf{S}_k(t_M)\exp(jk\omega_0 t_0)\right], \tag{4}$$

where t_0 and t_M are treated as two uncorrelated time variables (the fast carrier time and the slow modulation time) and $\mathbf{S}_k(t_M)$ is the time-dependent complex envelope (or modulation law) of the kth harmonic. The initial large-size HB numerical problem is then replaced by a sequence of N_M small-size HB systems, where N_M is the number of time instants used to sample the T_M period.

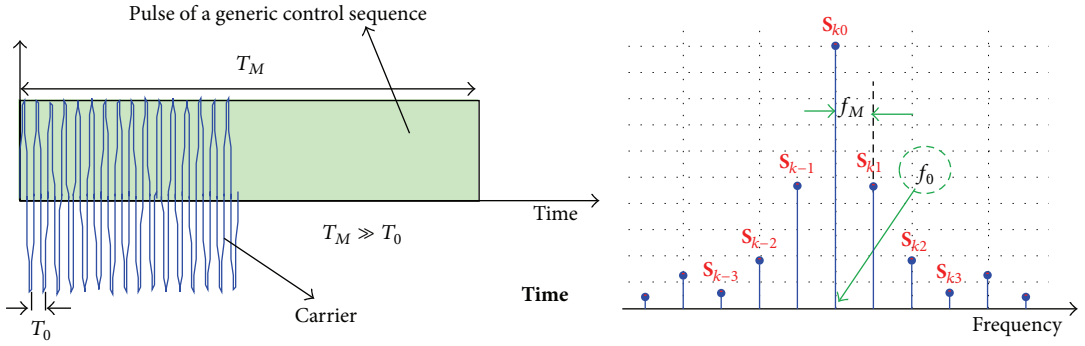

Figure 1: Time- and frequency-domain descriptions of the two-tone regime due to intermodulation of the RF carrier with the switch modulation frequency.

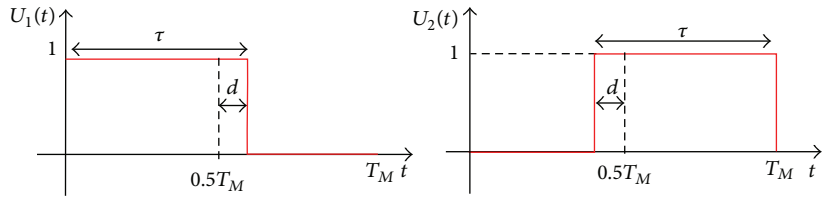

Figure 2: Periodic control sequences of the two inner elements of the array, providing Σ and Δ patterns.

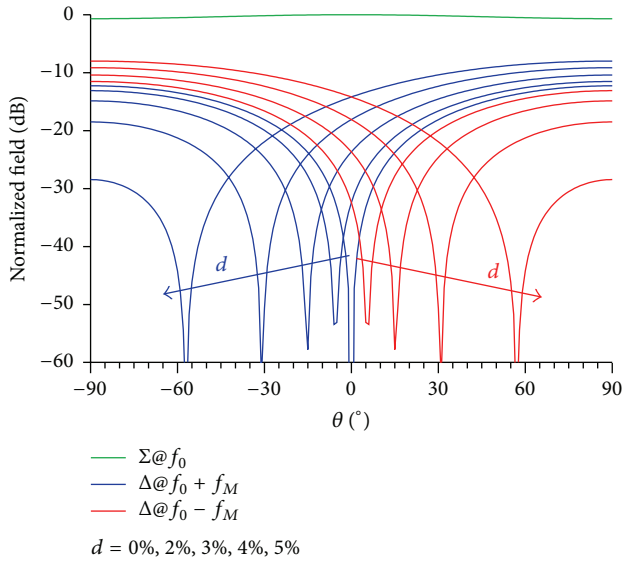

Figure 3: Fixed Σ and steerable Δ patterns of an array of two isotropic radiators with $\lambda/8$ spacing, as a function of the tuning parameter d.

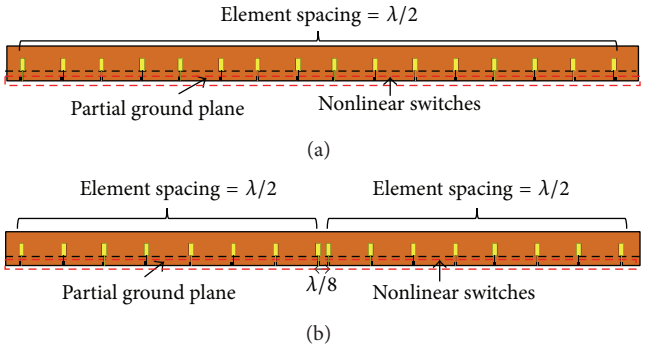

Figure 4: Linear TMA topologies with (a) equally spaced and (b) unequally spaced arrangements.

The evaluation of the far-field (1) may be carried out within the PHB-based CAD platform by exploiting the linearity of the antenna system. Let $I_1^{(i)}(t_M)$ be the complex envelope of the excitation current at the ith antenna port at the fundamental frequency f_0 ($k = 1$). The corresponding far-field envelope is given by

$$\begin{aligned}\mathbf{E}(r,\theta,\phi;t_M) &= \frac{\exp(-j\beta r)}{r} \\ &\cdot \sum_{i=1}^{n_A} \left[\hat{\boldsymbol{\theta}} B_\theta^{(i)}(\theta,\phi;\omega_0) + \hat{\boldsymbol{\phi}} B_\phi^{(i)}(\theta,\phi;\omega_0)\right] I_1^{(i)}(t_M) - j \\ &\cdot \frac{1}{r}\left[\sum_{i=1}^{n_A} \frac{\partial\left\{\exp(-j\beta r)\left[\hat{\boldsymbol{\theta}} B_\theta^{(i)}(\theta,\phi;\omega_0) + \hat{\boldsymbol{\phi}} B_\phi^{(i)}(\theta,\phi;\omega_0)\right]\right\}}{\partial\omega}\bigg|_{\omega=\omega_0}\right. \\ &\left.\cdot \frac{dI_1^{(i)}(t_M)}{dt_M}\right],\end{aligned} \tag{5}$$

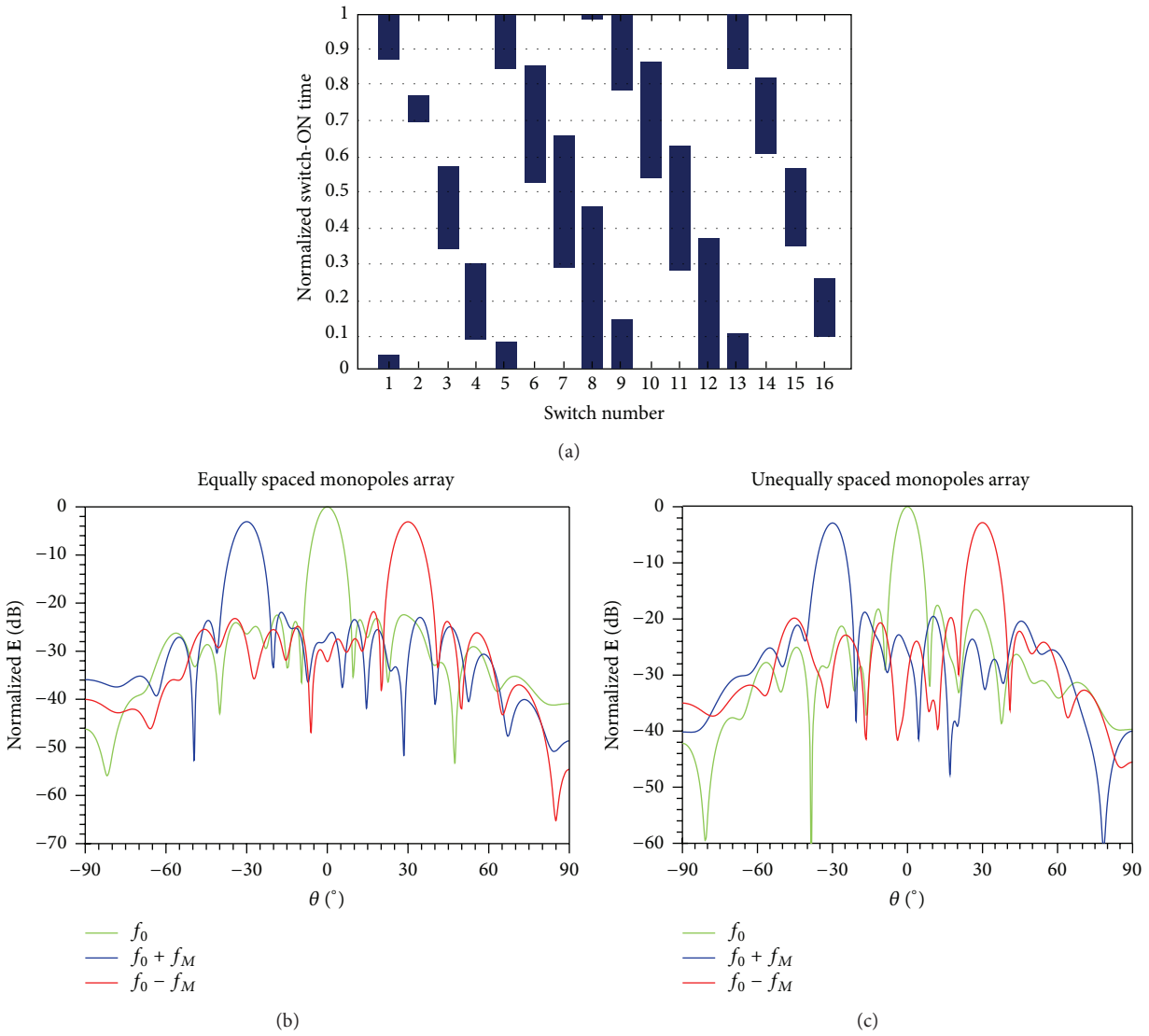

FIGURE 5: (a) Optimized control sequence for harmonic beamforming of an ideal 16-dipole uniform array [16]. Corresponding fundamental and first sidebands normalized radiation patterns for power transfer in $\theta = -30^\circ, 0^\circ, 30^\circ$ directions: (b) for the equally spaced array of Figure 4(a) and (c) for the unequally spaced array of Figure 4(b).

where $B_\theta^{(i)}$ and $B_\phi^{(i)}$ are the scalar components of the normalized field, directly obtained from a sequence of full-wave analyses. For each array port, the generic ith radiating element ($i = 1, \ldots, n_A$) is excited by a unit-amplitude sinusoidal current source of frequency f_0, while the other ports are left open. It is worth mentioning that for a given antenna topology this time-consuming electromagnetic (EM) database has to be evaluated only once in the frequency bands of interest and can then be reused in the analysis of any arbitrary antenna regime.

4. Time-Modulated Arrays for Wireless Power Transfer

The versatility of TMA systems described in Section 2 and the rigorous simulation platform discussed in Section 3 can now be exploited to develop an original efficient two-step procedure for describing power transmission to tagged sensors possibly equipped with rectifying antennas and randomly positioned in an indoor scenario.

The first step deploys the direction finding capability of a two-element array described in [8]. The use of driving sequences of the two diodes of the kind reported in Figure 2 results in the simultaneous presence of a sum (Σ) pattern (two elements in phase) and a difference (Δ) pattern (two elements 180° out of phase) at the fundamental (f_0) and at the first sideband harmonics ($f_0 \pm f_M$), respectively. As a further proof of TMA reconfigurability, a change of the duty cycle of the two symmetric excitations (by acting on the parameter d, shown in Figure 2) causes the steering of the Δ-pattern.

In order to improve the localization capabilities an element spacing of $\lambda/8$ is suggested in [8]. In this way a flatter Σ pattern is achieved, thus allowing a more constant array behavior while steering. This also indirectly explains why

a simple two-element array, instead of a more directive multielement array, is deployed in this phase.

For completeness, Figure 3 shows the Σ and Δ patterns of an array of two isotropic elements with $\lambda/8$ spacing, as a function of d.

The second step relies on the use of the entire TMA with several radiating elements, in order to increase the array directivity and thus to precisely energize the tags detected in the previous step.

The research activity on control sequences optimization available in the literature is uniquely devoted to standard uniform arrays, with half-wavelength spaced ideal elements (typically mathematical dipoles or isotropic radiators). In this paper we want to analyze the behavior of both uniform and nonuniform arrays, in order to investigate the localization performance by varying the spacing between the two inner elements of the array (as suggested in [8]). For this reason we first verify the effect of real radiating elements and of nonuniform feeding on TMA performance, while using optimized control sequences taken from the literature.

For this purpose we carry out a performance comparison between the two arrays reported in Figure 4. 16 planar monopoles realized on RF60A Taconic substrate ($\varepsilon_r = 6.15$, thickness = 0.635 mm) resonating at 2.45 GHz are arranged both in equally spaced (Figure 4(a)) and unequally spaced (Figure 4(b)) architectures. For the WPT application we have in mind that the harmonic beamforming feature [6, 7, 16] takes on a particular interest: for this reason we decide to test the switch excitation pattern taken from [16] and shown in Figure 5(a) in terms of duty cycle (switch-ON percentage of the modulation period). An envelope PHB analysis with $N_M = 1000$ sampling instants per modulation period (here and in the following, $T_M = 10\,\mu$s, $f_M = 100$ kHz) is carried out for both the equally and the unequally spaced arrays. The EM databases composed of the complex coefficients $B_\theta^{(i)}, B_\phi^{(i)}$ have to be extracted for both arrays in order to obtain the results shown in Figures 5(b) and 5(c), where the broadside pattern at the fundamental (f_0) and the patterns pointing in the $\theta = \pm 30^\circ$ directions at the first sideband harmonics ($f_0 \pm f_M$) are compared.

First of all, the radiation patterns of Figure 5(b) closely agree with those reported in [16]. Furthermore, some discrepancies between the equally and the unequally spaced array behavior can be detected by inspection of Figures 5(b) and 5(c). However, discrepancies are mainly limited to side lobes, showing a side lobe level (SLL) worsening of almost 5 dB for all the patterns in the unequally spaced case, while maintaining the main lobes shape and pointing direction. The previous results lead us to conclude the test by assuming that control patterns extracted from uniform (ideal) arrays can be successfully applied to real radiating uniform and (slightly) unequally spaced structures.

5. Step 1: TMA for Tag Localization

The software platform described in Section 3 allows us to compare the performance of different subarray layouts for the localization phase. Note that the EM database, $B_\theta^{(i)}, B_\phi^{(i)}$, previously obtained for each 16-port array is used for this kind of analysis, too: therefore, the actual EM couplings between nearby elements are rigorously taken into account.

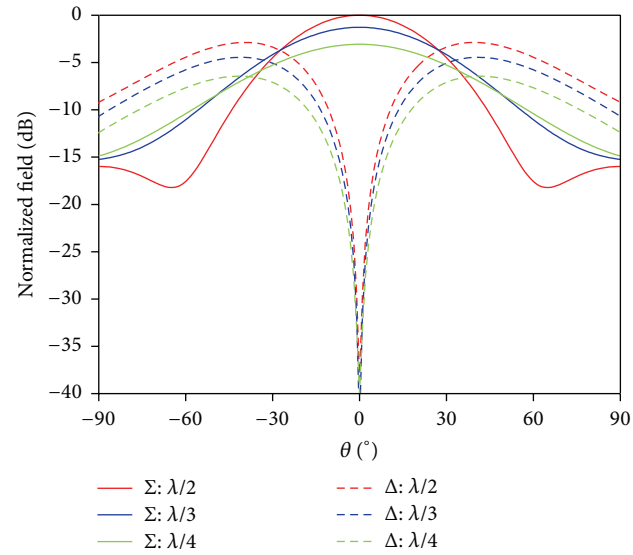

Figure 6: Σ and Δ patterns of the two inner patches of subarray for different antenna spacing.

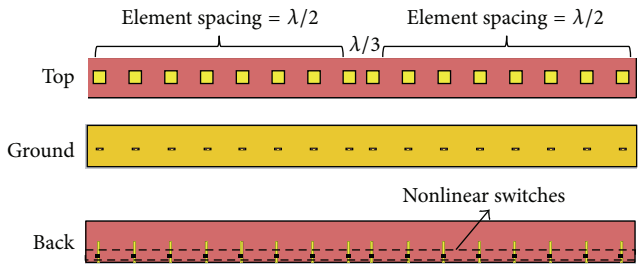

Figure 7: Unequally spaced linear TMA multilayer topology with planar square patch antennas.

5.1. Two-Element Subarray Topology Selection. In addition to the two array topologies shown in Figure 4, we want to test the behavior of a standard planar patch array, too, still operating at 2.45 GHz. A rectangular aperture in the ground plane is used to excite each square patch through a backside feeding line, both realized on RF60A Taconic substrate. The more directive behavior of the patch antenna compared to the previous monopole case suggests investigating the effect of the two inner patches' distance on the Σ and Δ patterns. We simply limit this investigation to full-wave simulations of the entire 16-element array, with excitations provided to the couple of central elements only. The $\lambda/2$, $\lambda/3$, and $\lambda/4$ spacing cases are compared in Figure 6 (further spacing reduction is not feasible, due to square patch geometry). The expected less flat Σ behavior in the scanning (horizontal) plane of the $\lambda/2$ spacing case suggests giving up this choice. On the contrary, there is no significant difference between the two closer arrangements. We thus decide to include the unequally

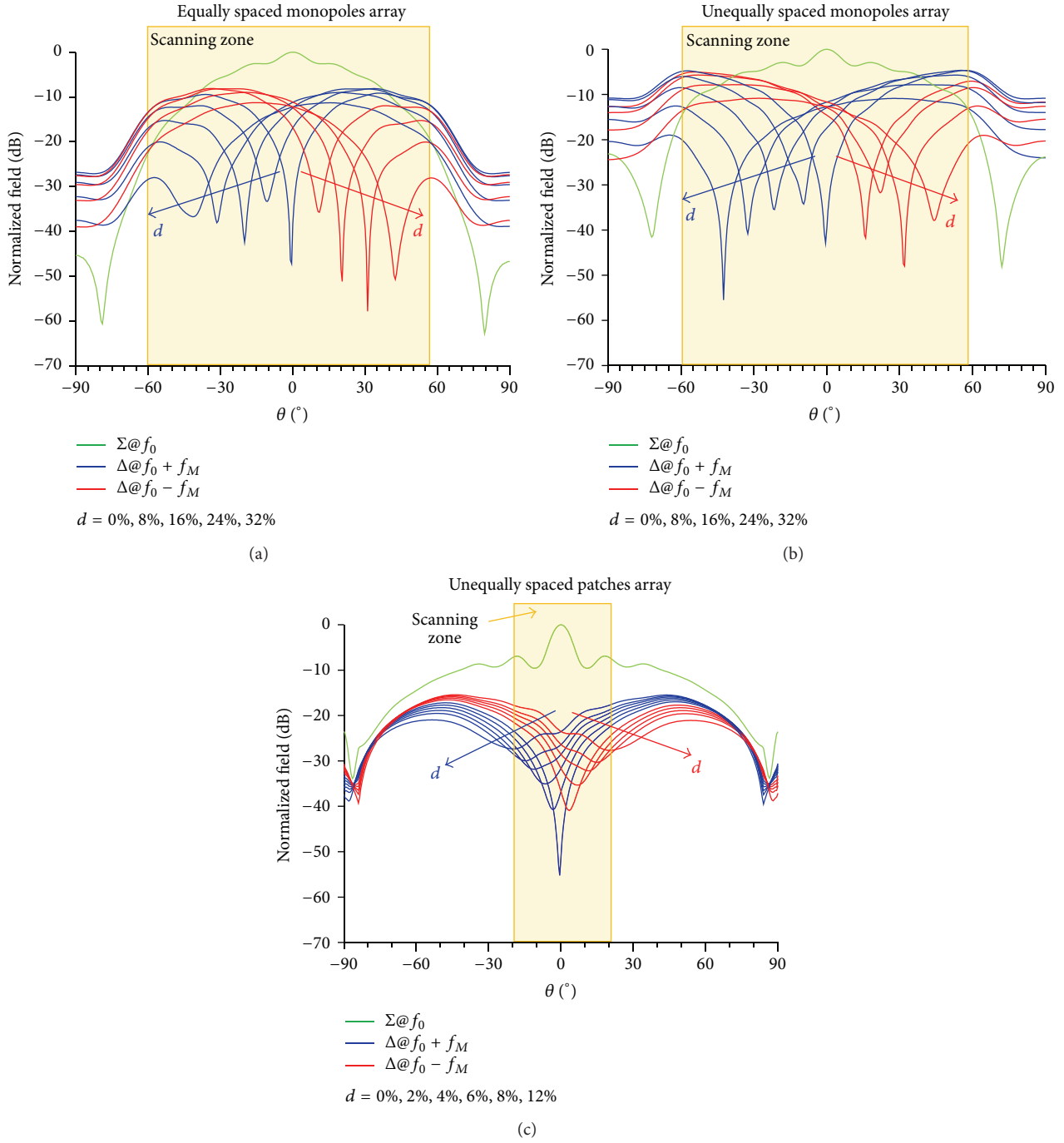

FIGURE 8: Scanning performance comparison between the two inner elements of subarrays of the TMAs: (a) of Figure 4(a); (b) of Figure 4(b); and (c) of Figure 7.

spaced patch array topology with $\lambda/3$-inner element spacing of Figure 7 in the following investigation, too.

At this stage, several envelope PHB analyses are carried out with the 14 peripheral switches left open and the two inner ones driven by the sequences reported in Figure 2, for different d values. Figures 8(a), 8(b), and 8(c) report the fixed Σ pattern and the steered Δ patterns for the arrays of Figures 4(a), 4(b), and 7, respectively.

It is interesting to note the almost equivalent behavior of the two monopole arrays. The unequally spaced version exhibits a slightly flatter Σ pattern, as expected, and marginally sharper Δ nulls in the side regions of the scanning zone. These plots also prove that real-world antennas need more asymmetric driving sequences (higher d values) for Δ pattern steering, if compared with isotropic radiators (Figure 3).

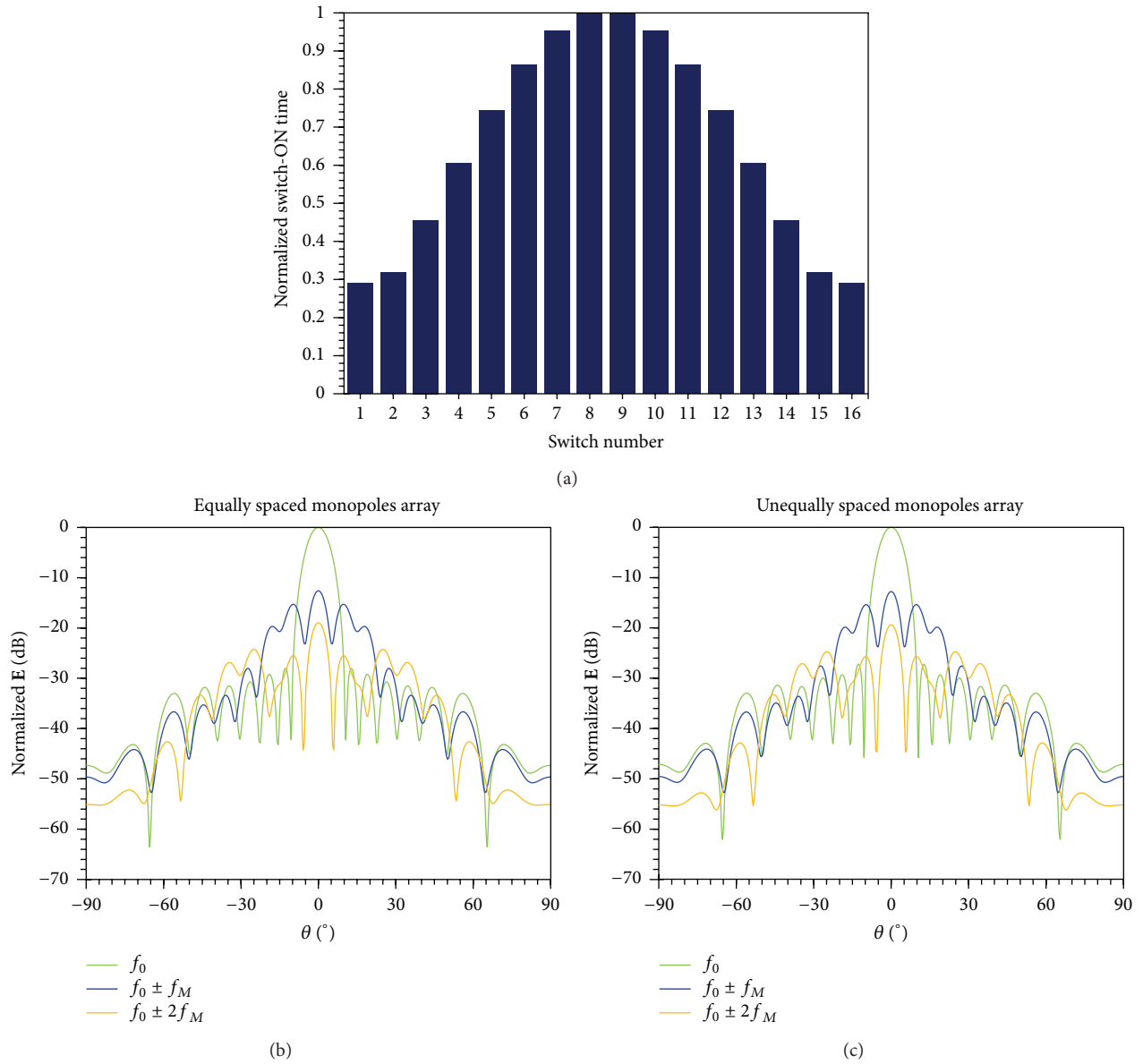

Figure 9: (a) Control sequence reproducing a Dolph-Chebyshev pattern with SLL = −30 dB; corresponding fundamental and first two harmonics normalized radiation patterns for broadside power transfer with (b) the TMA of Figure 4(a) and (c) the TMA of Figure 4(b).

As regards the patch array, the shape of the Δ patterns is still good, but for small d values only. Indeed, an increase in the value of d leads to a rapid degradation of the Δ pattern for even smaller d values than in the monopole case. The overall scanning zone is more than halved with respect to the monopole arrays: that is, the more directive behavior of patch antennas is a limiting factor for this application.

These comparisons allow us to conclude that 16-monopole arrays both equally and unequally spaced are suitable for the smart WPT operation under exam, since a significant scanning region $\theta \in [-60^\circ; 60^\circ]$ is available in both cases.

5.2. Tag Localization. Once the tags have been interrogated by the TMA array, they reply by taking the power supply either from their onboard rechargeable battery (active tags) or from rectification of the incoming RF signal (passive tags). In both cases the sharp nulls of the steered Δ patterns represent the key issue in tag detection. The combination of the Received Signal Strength Indicators (RSSI) coming from the tags, due to the Σ and Δ patterns of the receiving array, allows us to compute the Maximum Power Ratio (MPR) [19], defined as

$$\mathrm{MPR}(\theta) = \Sigma^{\mathrm{dB}}_{\mathrm{RSSI}}(\theta) - \Delta^{\mathrm{dB}}_{\mathrm{RSSI}}(\theta). \quad (6)$$

The information provided by (6), in conjunction with the scanning capability, has proven its effectiveness in indoor localization. Resolutions up to few cm at a reader-to-tag distance of 3 m, for a two-element 2.45 GHz array, have been achieved [19].

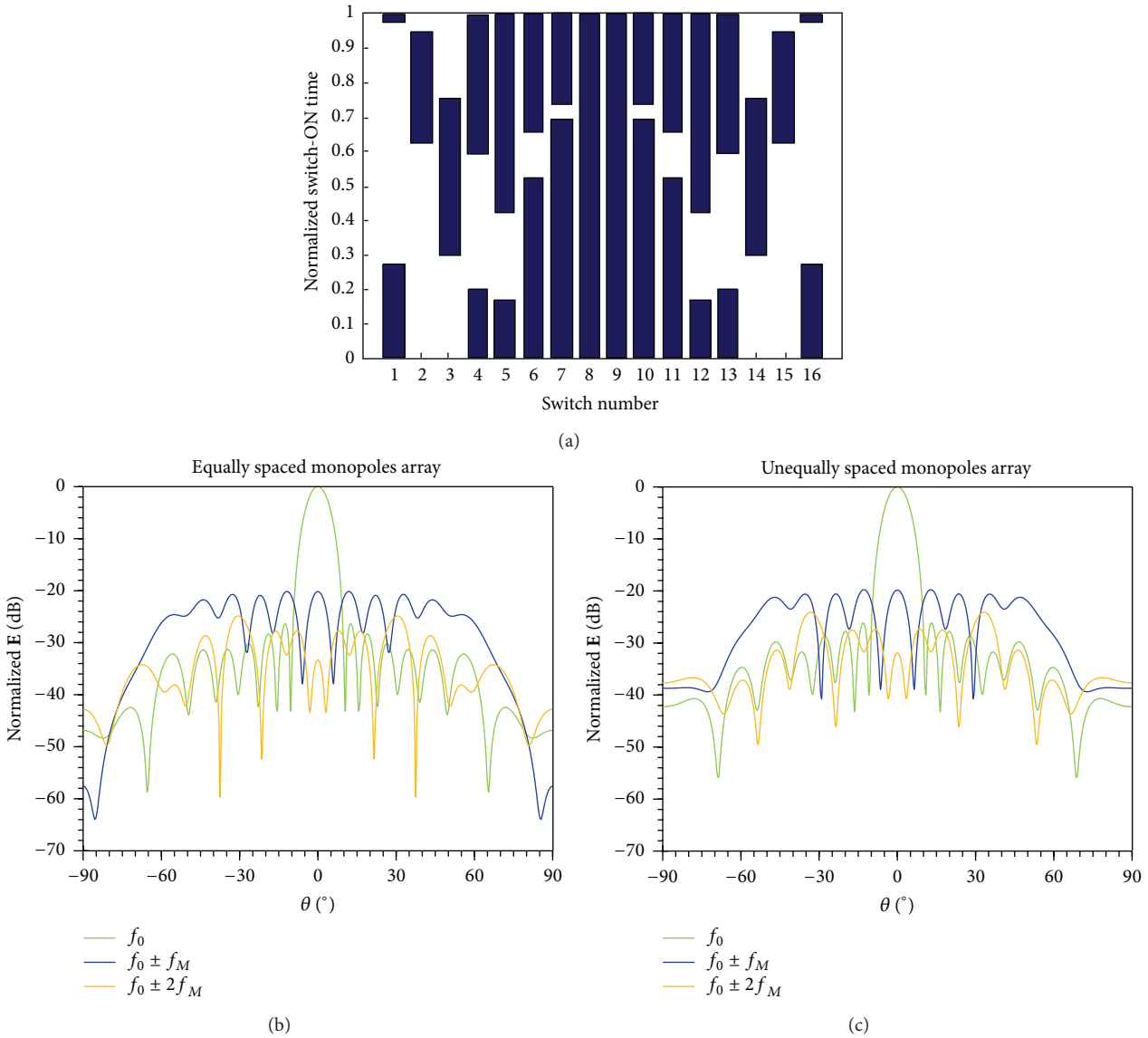

FIGURE 10: (a) Control sequence providing SLL = −30 dB and sideband radiation = −20 dB [11]; corresponding fundamental and first two harmonics normalized radiation patterns for broadside power transfer with (b) the TMA of Figure 4(a) and (c) the TMA of Figure 4(b).

At the end of the localization phase a vector of N_{tag} values of θ corresponding to the peaks of the received MPRs (θ_{peak}) is recorded, and the second step of the WPT procedure can take place.

6. Step 2: Power Transfer

Once the tag positions have been detected, all the 16 nonlinear switches are biased by proper control sequences, in such a way as to precisely point the array beams in the desired directions. In this phase a possible mode of operation can split the scanning region ($\theta \in [-60^\circ \div 60^\circ]$) into sectors of amplitudes equal to the 16-element array half power beam width (HPBW) (7° in this case). For each θ_{peak} falling in the sector centered around θ_{HPBW}, a preloaded control sequence allowing us to point the fundamental or sideband harmonics beam into the θ_{HPBW} direction is adopted to bias the switches.

As a first application example, the case of a single tag in the broadside direction ($\theta = 0^\circ$) is considered. An easy way to reach this goal is to adopt a control sequence reproducing a Dolph-Chebyshev excitation pattern in the time domain. Figure 9(a) shows the switch-ON pattern providing an SLL of −30 dB. The problem with this type of excitation, where all the switches share the same ON instant, is the high level of sideband radiation. This aspect is evident from Figure 9(b), showing the normalized radiation patterns of the TMA of Figure 4(a) at the fundamental and at the first and second harmonics. The power transmitted at the sideband harmonics is significant, even in directions different from the broadside one. Almost identical results are obtained from a similar simulation of the unequally spaced array of Figure 4(b), as shown in Figure 9(b).

When it comes to energy-aware solutions, a more focused power transmission is required. Indeed, in order to avoid

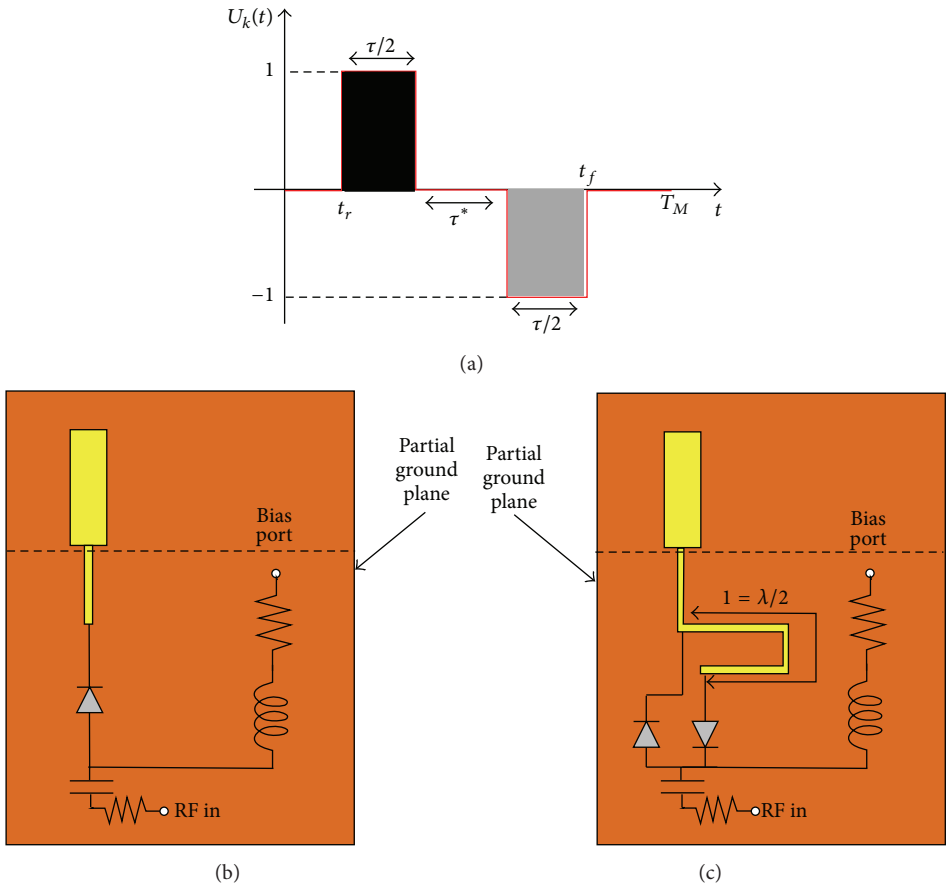

Figure 11: (a) Control sequence with zero mean value; detail of bias and feed networks of the planar monopole antenna (b) for standard positive rectangular pulse sequences and (c) for zero mean value sequences.

wasting power we need to suppress the sideband radiation while preserving a good SLL. In Figure 10(a) we report the switch-ON pattern taken from [11], in which the switch-ON instant becomes an additional degree of freedom in the optimization process. Figure 10(b) reports the corresponding simulated normalized radiation patterns at the frequencies of interest. SLL below −30 dB and sideband radiation below −20 dB are achieved. Very similar results have been obtained with the same sequence applied to the unequally spaced array of Figure 4(b), as demonstrated by Figure 10(c).

The more complex scenario of three detected tags inside the sectors centered around $\theta_{\text{HPBW}} = -30^\circ, 0^\circ$, and 30° can finally exploit the harmonic radiation, since the previously discussed control sequence and radiation patterns (see Figures 5(a), 5(b), and 5(c)) allow us to simultaneously energize the desired tags.

In those scenarios where the tags to be energized do not fall in the $\theta_{\text{HPBW}} = 0^\circ$ sector, the versatility of TMAs allows us to avoid wasting additional power by switching off the radiation pattern at the fundamental frequency. This further result can be obtained by means of the new kind of control sequences we propose in Figure 11(a): the zero mean value of the symmetric periodic waveform automatically cancels radiation at f_0, as can be easily shown by evaluating of the Fourier coefficient u_{0p} in (2). It is worth noting that these symmetric sequences introduce a further degree of freedom that can be exploited in the design process, namely, the time interval τ^* between the positive and negative pulses. This kind of sequence needs a more complex circuital solution, because the suitable excitation of the antenna port can be reached by adopting a pair of antiphase switches which are driven by the positive and by the negative pulses, respectively. In Figures 11(b) and 11(c) the detailed view of a generic monopole is shown, for both a traditional and a zero mean value sequence, respectively. An additional half wavelength-long meandered line connected to the switch driven by the negative pulse allows us to have in-phase currents at the antenna port.

According to this new solution a symmetric radiation pattern involving only the sideband harmonics $f_0 \pm f_M$ can be obtained, as confirmed by the results of Figure 12. The suboptimal control sequence (with $\tau^* = 0$) of Figure 12(a) has been obtained by us by means of a MATLAB optimization of a uniform ideal array, with the design constraint of SLL = −30 dB. The corresponding nonlinear/EM envelope PHB cosimulation of the uniform array produces the two sideband maxima of Figure 12(b) in correspondence of the sectors $\theta_{\text{HPBW}} = \pm 21^\circ$, with absence of radiation at f_0. This new type of control pattern seems to be more sensitive to the unequal spacing of the array elements as in Figure 4(b), as

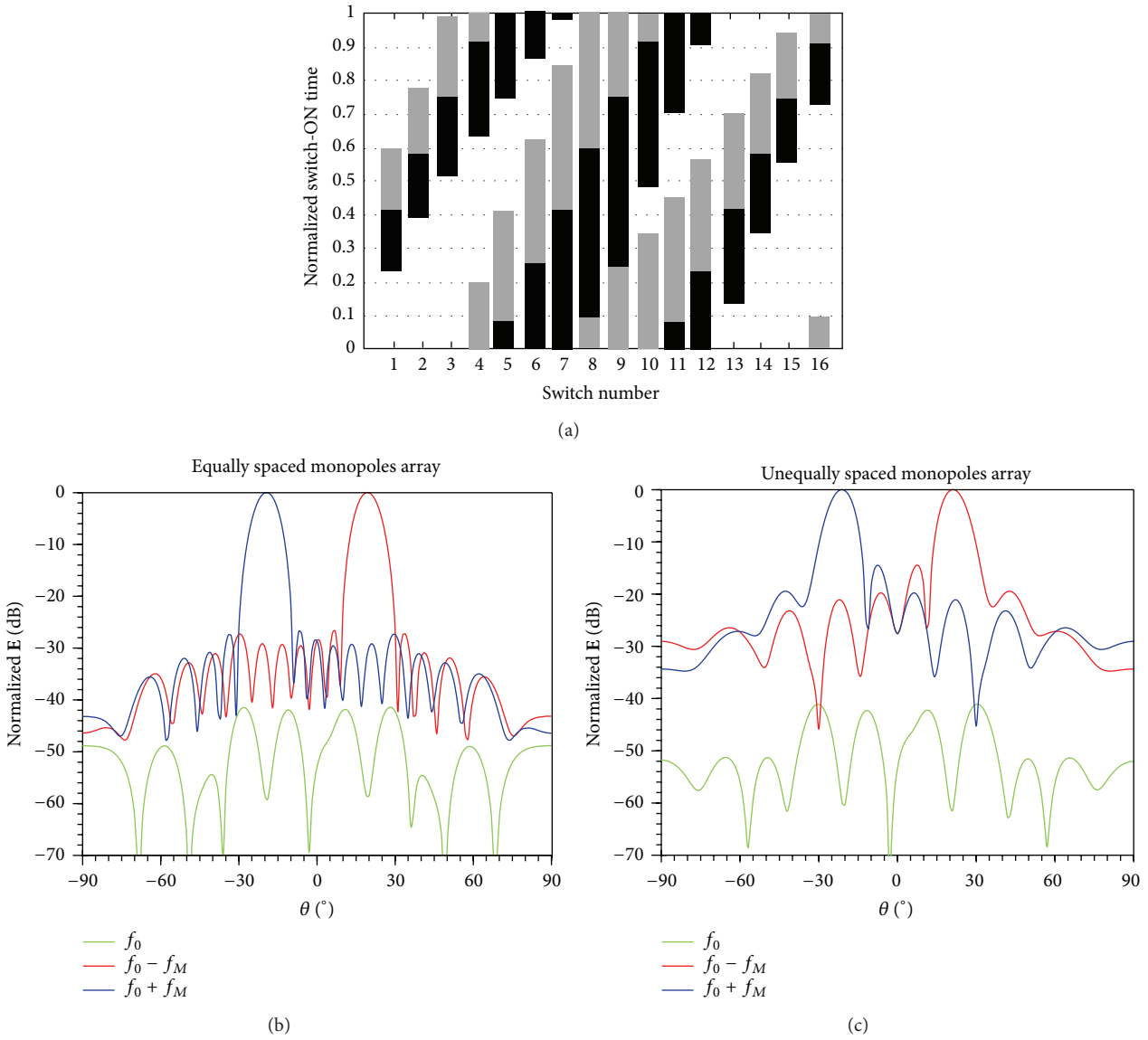

FIGURE 12: (a) Control pulse with null mean value (with black and gray time slots for positive and negative pulses, resp.); corresponding fundamental and first sidebands normalized radiation patterns for power transfer in $\theta = \pm 21^{\circ}$ directions (b) for the TMA of Figure 4(a) and (c) for the TMA of Figure 4(b).

shown by the plots of Figure 12(c): the maximum radiation directions are preserved, but the SLL is significantly deteriorated. Sequence optimization taking into account the actual array layout will thus be useful for future high-precision TMA applications.

7. Conclusion

In this paper, we present a new dynamic two-step WPT function deploying the versatility of TMAs. The unrivaled level of reconfigurability of TMA due to almost unlimited choice of control patterns driving the nonlinear switches permits us to detect and precisely energize randomly placed sensors. The adopted numerical approach is based on the combination of HB-based circuit-level analysis techniques and full-wave EM analysis, thus automatically taking into account the actual switch dynamics and the unavoidable antenna couplings. This approach allows us to rigorously handle the complex simulation of the modulated field vector radiated by a planar TMA, and, for this reason, it should be combined with control sequence optimization processes in order to increase the overall system design accuracy. The interesting results produced together with the ease of TMA implementation make these radiating systems adequate for modern wireless applications.

Conflict of Interests

The authors declare that there is no conflict of interests regarding the publication of this paper.

References

[1] W. Kummer, A. Villeneuve, T. Fong, and F. Terrio, "Ultra-low sidelobes from time-modulated arrays," *IEEE Transactions on Antennas and Propagation*, vol. 11, no. 6, pp. 633–639, 1963.

[2] S. Yang, Y. B. Gan, and A. Qing, "Sideband suppression in time-modulated linear arrays by the differential evolution algorithm," *IEEE Antennas and Wireless Propagation Letters*, vol. 1, pp. 173–175, 2002.

[3] L. Poli, P. Rocca, and A. Massa, "Sideband radiation reduction exploiting pattern multiplication in directive time-modulated linear arrays," *IET Microwaves, Antennas & Propagation*, vol. 6, no. 2, pp. 214–222, 2012.

[4] C. He, H. Yu, X. Liang, J. Geng, and R. Jin, "Sideband radiation level suppression in time-modulated array by nonuniform period modulation," *IEEE Antennas and Wireless Propagation Letters*, vol. 14, pp. 606–609, 2015.

[5] L. Poli, P. Rocca, G. Oliveri, and A. Massa, "Adaptive nulling in time-modulated linear arrays with minimum power losses," *IET Microwaves, Antennas & Propagation*, vol. 5, no. 2, pp. 157–166, 2011.

[6] Y. Tong and A. Tennant, "Simultaneous control of sidelobe level and harmonic beam steering in time-modulated linear arrays," *Electronics Letters*, vol. 46, no. 3, pp. 201–202, 2010.

[7] G. Li, S. Yang, Y. Chen, and Z. Nie, "A novel electronic beam steering technique in time modulated antenna arrays," *Progress in Electromagnetics Research*, vol. 97, pp. 391–405, 2009.

[8] A. Tennant and B. Chambers, "A two-element time-modulated array with direction-finding properties," *IEEE Antennas and Wireless Propagation Letters*, vol. 6, pp. 64–65, 2007.

[9] G. Li, S. Yang, and Z. Nie, "Direction of arrival estimation in time modulated linear arrays with unidirectional phase center motion," *IEEE Transactions on Antennas and Propagation*, vol. 58, no. 4, pp. 1105–1111, 2010.

[10] C. He, X. Liang, Z. Li, J. Geng, and R. Jin, "Direction finding by time-modulated array with harmonic characteristic analysis," *IEEE Antennas and Wireless Propagation Letters*, vol. 14, pp. 642–645, 2015.

[11] L. Poli, P. Rocca, L. Manica, and A. Massa, "Pattern synthesis in time-modulated linear arrays through pulse shifting," *IET Microwaves, Antennas & Propagation*, vol. 4, no. 9, Article ID IMAPCH000004000009001157000001, pp. 1157–1164, 2010.

[12] J. Yang, W.-T. Li, X.-W. Shi, L. Xin, and J.-F. Yu, "A hybrid ABC-DE algorithm and its application for time-modulated arrays pattern synthesis," *IEEE Transactions on Antennas and Propagation*, vol. 61, no. 11, pp. 5485–5495, 2013.

[13] J. Euziere, R. Guinvarc'h, B. Uguen, and R. Gillard, "Optimization of sparse time-modulated array by genetic algorithm for radar applications," *IEEE Antennas and Wireless Propagation Letters*, vol. 13, pp. 161–164, 2014.

[14] D. Masotti, P. Francia, A. Costanzo, and V. Rizzoli, "Rigorous electromagnetic/circuit-level analysis of time-modulated linear arrays," *IEEE Transactions on Antennas and Propagation*, vol. 61, no. 11, pp. 5465–5474, 2013.

[15] Y. Li and V. Jandhyala, "Design of retrodirective antenna arrays for short-range wireless power transmission," *IEEE Transactions on Antennas and Propagation*, vol. 60, no. 1, pp. 206–211, 2012.

[16] L. Poli, P. Rocca, G. Oliveri, and A. Massa, "Harmonic beamforming in time-modulated linear," *IEEE Transactions on Antennas and Propagation*, vol. 59, no. 7, pp. 2538–2545, 2011.

[17] V. Rizzoli, D. Masotti, F. Mastri, and E. Montanari, "System-oriented harmonic-balance algorithms for circuit-level simulation," *IEEE Transactions on Computer-Aided Design of Integrated Circuits and Systems*, vol. 30, no. 2, pp. 256–269, 2011.

[18] CST Microwave Studio 2013, http://www.cst.com/.

[19] M. Del Prete, D. Masotti, N. Arbizzani, and A. Costanzo, "Remotely identify and detect by a compact reader with monopulse scanning capabilities," *IEEE Transactions on Microwave Theory and Techniques*, vol. 61, no. 1, pp. 641–650, 2013.